Tanzania Journal of Science 49(4): 809-818, 2023
ISSN 0856-1761, e-ISSN 2507-7961

Impact of Zn and W Doping Levels on Properties of Thermochromic VO_2-Based Thin Films

Haji F Haji[1,2*], Margaret E Samiji[1] and Nuru R Mlyuka[1]
[1]*Department of Physics, University of Dar es Salaam, P.O. Box 35063, Dar es Salaam, Tanzania.*
[2]*Department of Natural Sciences, The State University of Zanzibar, P.O. Box 146, Zanzibar, Tanzania.*
**Corresponding author, e-mail: haji.faki@suza.ac.tz*
Received May 2023, Revised 8 Aug 2023, Accepted 29 Aug 2023 Published Oct 2023
DOI: https://dx.doi.org/10.4314/tjs.v49i4.3

Abstract

DC magnetron sputtering at a substrate temperature of 425 °C was used to successfully deposit W/Zn-doped VO_2 thin films on soda lime glass (SLG) substrates. The aim was to investigate the influence of Zn doping levels on the transition temperature (τ_c), luminous transmittance (T_{lum}) and solar transmittance modulation (ΔT_{sol}) of VO_2-based thin films. UV/VIS/NIR spectrometer, X-ray Diffraction (XRD), Atomic Force Microscope (AFM), and Rutherford Backscattering Spectroscopy (RBS) were used to characterise the thin films. It was revealed that W/Zn co-doped VO_2 thin films with ~10.8 at.% Zn showed a luminous transmittance of ~40.4%, with excellent solar transmittance modulation of 10.2%. Furthermore, the transition temperature obtained for the Zn and W co-doped VO_2 films with ~ 10.8 at.% Zn was lower at 23.1 °C compared to 25.6 °C and 26.8 °C for thin films with ~3.9 at.% Zn and ~2.8 at.% Zn, respectively. It was not possible to deposit the films with Zn doping level above 10.8 at.% due to some technical limitations. These findings indicate that thin films with a controlled proportion of Zn in the W/Zn co-doped VO_2-based thin films have the potential to be employed for applications such as smart windows.

Keywords: W/Zn co-doping, Vanadium dioxide; Co-sputtering, Smart windows.

Introduction

The structural change of bulk VO_2 from semiconducting to metallic phase at a transition temperature, τ_c, of ~68 °C has attracted a lot of interest due to a number of potential technological applications (Mlyuka et al. 2009, Guo et al. 2021, Zhang et al. 2021). It has been noted that thin films of VO_2 are highly transparent below τ_c, especially in the near-infrared region of the solar spectrum, but strongly reflective above τ_c (Mussa et al. 2018). In light of this, VO_2 has great potential to be used as a smart window coating that can regulate solar transmittance into and out of architectural buildings in accordance with ambient temperature and comfort requirements (Haji and Mlyuka 2015). However, in order to achieve the requirements for useful smart windows, three fundamental challenges need to be addressed. These challenges include too-high transition temperature (τ_c), low luminous transmittance (T_{lum}), and solar transmittance modulation (ΔT_{sol}) (Li et al. 2012, Li et al. 2013).

Several efforts have been made to reduce τ_c and improve T_{lum} and ΔT_{sol}. The use of multilayer structures and elemental doping, as well as modifying structures, and the choice of various substrates, are some of these efforts (Mlyuka et al. 2009, Wang et al. 2016). Out of these efforts, elemental doping

is reported to be a significant approach for improving the thermochromic properties of VO_2-based thin films. So far, several dopants have been attempted and shown significant effects on thermochromic properties of VO_2 thin films. These include W (Batista et al. 2009, Mao et al. 2014, Karaoglan-Bebek et al. 2014, Liu et al. 2016, Dou et al. 2018), Mo (Khan et al. 2017), Nb (Batista et al. 2011), Mg (Granqvist et al. 2010, Gagaoudakis et al. 2016), and Al (Lyobha et al. 2018, Ji et al. 2018). The incorporation of W in VO_2 films has the greatest impact on τ_c reduction of VO_2 based thin films out of the several dopants that have been studied (Liu et al. 2016). However, W doping has been reported to compromise both T_{lum} and ΔT_{sol} of VO_2-based thin films (Mlyuka 2010, Huang et al. 2020). Therefore, it is still an issue to effectively lower τ_c for the phase change between monoclinic and rutile phases of VO_2 without compromising T_{lum} and ΔT_{sol}. One way to achieve this is to combine W doping with other dopants that might positively influence T_{lum} and ΔT_{sol}.

Dopant combinations, including those of W and Al have also been reported to improve both T_{lum} and ΔT_{sol} of VO_2 films; however, τ_c was found to increase with increasing Al doping concentration (Lyobha et al. 2018). On top of that, Mg has also been co-doped with W in VO_2 films and found to improve T_{lum} but τ_c reduction was not significant (Wang et al. 2015). Indeed, W and Zn co-doping to VO_2-based thin films has been attempted very recently, and promising results, especially on enhanced T_{lum} with a reasonable τ_c value have been reported (Haji et al. 2023). But the influence of W and Zn doping levels on VO_2-based thin films has not been fully explored for smart window coatings. Therefore, the present work reports on the combined effect of W and Zn doping levels on the thermochromic properties of VO_2-based thin films.

Materials and Methods

Reactive DC magnetron sputtering was used to deposit the W/Zn co-doped VO_2 thin films on top of soda lime glass (SLG) substrates by co-sputtering V(99)W(01) at.% alloy target and pure Zn target (99.9% purity) both supplied by Plasmaterials Company (2268 Research Drive, Livermore, CA 94550-USA). The supplied targets had a dimension of 2-inch diameter by 0.250-inch thick. The target to substrate distance in the chamber was maintained at 14.5 cm. The chamber base pressure was 9.4×10^{-6} mbar, and the temperature on the substrate was maintained at 425 °C. The working pressure was maintained at 4.7×10^{-3} mbar by controlling the manual gate valve between the chamber and the turbo-molecular pump, and the flow rates of argon (99.999%) and oxygen (99.9%) were 75 ml/min and 4.23 ml/min, respectively. To obtain films with different Zn dopant levels, different sputtering powers of 10 W, 15 W, and 20 W were applied to the Zn target. The Tencor Alpha Step IQ surface profiler later confirmed the thickness of the films that were estimated based on the deposition rates. Transmittances of the W/Zn co-doped VO_2-based thin films were measured using a PerkinElmer lambda 1050+ UV/VIS/NIR spectrometer, and the integrated luminous and solar transmittance were estimated using Equation 1.

$$T_{lum,sol}=\frac{\int\phi_{lum,sol}(\lambda)T(\lambda)d\lambda}{\int\phi_{lum,sol}(\lambda)d\lambda} \quad (1)$$

where ϕ_{lum} is the standard luminous efficiency function for the photonic vision of human eyes, $T(\lambda)$ is spectral transmittance, and ϕ_{sol} is the solar irradiance spectrum for air mass 1.5 (corresponding to the sun standing 37° above the horizon). ΔT_{sol} is obtained as per Equation 2.

$$\Delta T_{sol}=T_{sol,25^{\circ}C}-T_{sol,100^{\circ}C} \quad (2)$$

The transmittance of the samples was taken at room temperature, corresponding to the semiconducting phase and 100 °C, corresponding to the metallic phase of VO_2-based thin films. The W/Zn co-doped VO_2 thin film samples were also characterized by X-ray diffractometer (XRD) to identify phases on the samples. Cu K-Alpha X-ray

radiation with a wavelength of 0.1504 nm was used in continuous scanning measurement mode with 2θ scanning range of 5° to 80°. W/Zn co-doped VO_2 films' surface morphology was examined using an atomic force microscope (AFM) in taping mode with a 1.960 Hz scan rate and a 1.00 μm scan size using the Digital Instruments Nanoscope (R) IIIa multimode AFM. The resulting AFM images were then examined for parameters related to grain distribution and roughness using Gwydion and *WSxM* software. Rutherford Backscattering Spectroscopy (RBS) was performed using 2.8 MeV ^{4}He (2+) ions to identify the dopants with their concentration levels at a scattering angle of 150°.

Results and Discussion

XRD analysis of W/Zn co-doped VO_2-based thin films

The x-ray diffraction spectra of W/Zn co-doped VO_2-based thin films are presented in Figure 1. For all the W/Zn co-doped VO_2 based thin film samples, diffraction peaks were observed at 2θ angles of 28.2°, 39.7°, 44.2°, 58.1°, and 71.9° corresponding to reflection planes (2 0 1), (0 0 2), ($\bar{2}$ 0 2), (4 0 2) and (3 3 2), respectively of VO_2 (M) phase based on the reference datasheet PDF# 33-1441. Neither W nor Zn metal or their corresponding oxides were observed in the spectra indicating that the VO_2 structure did not change with doping. The diffraction peak at 2θ equivalent to 39.7° with reflection plane (0 0 2) was found to be a dominant one indicating the preferred orientation of the crystallites, though the intensity was observed to increase with an increase in Zn concentration. Using Gaussian fit, the values of FWHM for the dominant XRD peak were determined and showed a slight spectral broadening for the films with relatively higher Zn doping levels compared to the films with lower Zn doping levels (Table 1). As the doping levels increase, the crystal lattice of VO_2-based thin films may be distorted leading to the presence of smaller crystallites (Burkhardt et al. 2002), which contribute to broadening of XRD peaks due to finite size of the crystalline domain. Lattice constants for the film with ~2.8 at.% Zn doping level were relatively smaller as compared to the films with ~3.9 at.% Zn and ~10.8 at.% Zn dopant levels, and in fact, similar effects were observed for inter-planer distance of the samples, at which the inter-planer distance for the film with a relatively lower Zn dopant was slightly lower compared to that with a higher Zn concentration in VO_2-based thin films. An increase in lattice constants of the VO_2-based thin films with increase in Zn doping level might be attributed to the lattice strain. The strain reduction along lattice parameters improves the stability of rutile VO_2 metallic phase and hence reduce the τ_c (Yu et al. 2020, Haji et al. 2023) The samples inter-planer distance, *d* and lattice constants *a*, for the peak corresponding to (0 0 2) planes were calculated based on the equations $n\lambda = 2d\sin 2\theta$ and $d_{hkl} = a/\sqrt{(h^2+k^2+l^2)}$, respectively, where *h*, *k*, *l* are the Miller indices of the lattice plane, *n* is an integer, and λ is the X-ray radiation wavelength, and θ is the Bragg's diffraction angle in degrees.

Table 1: FWHM, peak position (2θ), planar distance (d), and lattice constants (a) for W/Zn co-doped VO_2 based thin films with different doping levels of Zn

W/Zn co-doped VO_2 based thin films	FWHM (°)	2θ (°)	d (Å)	a (Å)
~2.8 at.% Zn	0.00334	39.63476	0.9151	1.8302
~3.9 at.% Zn	0.38909	39.55655	0.9466	1.8932
~10.8 at. %Zn	0.39153	39.55781	0.9830	1.9660

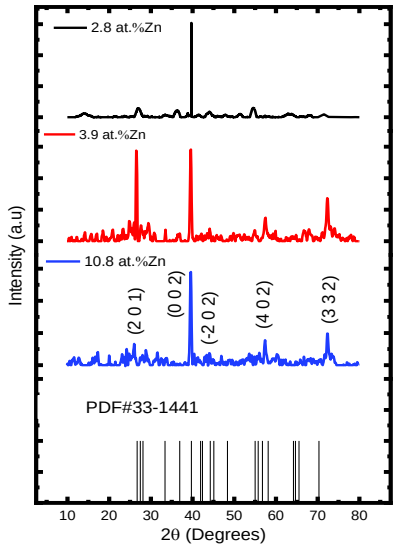

Figure 1: The XRD pattern of 96 nm thick W/Zn co-doped VO_2 thin films exhibits several peaks that are consistent with the monoclinic VO_2 structure for various Zn doping levels (2.8 at. % Zn, 3.9 at. % Zn and 10.8 at. % Zn).

AFM analysis of W/Zn co-doped VO_2-based thin films

Clusters of grains for W/Zn co-doped VO_2-based thin films with different Zn dopant concentrations are shown in Figure 2. The images reveal that, the grains for the sample with ~2.8 at.% Zn doping level (Figure 2 a, d, g), were relatively higher compared to the samples with ~3.9 at.% Zn and ~10.8 at.% Zn doping levels. AFM analysis also revealed a relatively higher mean roughness and RMS roughness for the W/Zn co-doped VO_2-based sample with ~2.8 at.% Zn compared to the samples with ~3.9 at.% Zn and ~10.8 at.% Zn dopant as presented in Table 2. Table 2 also indicates measures of deviation relative to the normal height distribution of thin film samples presented as the sample's skewness. The thin film with ~3.9 at.% Zn doping level showed relative higher skewness value of ~3.4 compared to ~1.2 and ~0.14 for the film with ~10.8 at.% Zn and ~2.8 at.% Zn, respectively. The kurtosis measures the sharpness or tailedness of the height distribution value. Thin film samples with ~3.9 at.% Zn doping level showed a relatively higher kurtosis value of ~22.6 compared to 5.6 and -1.3 for the samples with ~10.8 at.% Z n and ~2.8 at.% Zn, respectively (Table 2). Meaning that surface height of the samples with ~3.9 at.% Zn and ~10.8 at.% Zn doping levels was determined by more peaks and valleys while the sample with ~2.8 at.% Zn dopant level had fewer peaks and valleys. Furthermore, the sample's average height was observed to decrease with an increase in Zn concentration (Figure 3) as summarized in Table 2.

Table 2: Statistical parameters for the AFM measurements of W/Zn co-doped VO_2-based thin films

Zn doping level	RMS roughness (Sq)	Mean roughness (Sa)	Surface skewness (Ssk)	Surface kurtosis	Average height (nm)	Maximum value (nm)
2.8 at.% Zn	7.4724	6.0264	0.1369	-1.27111	27.7979	53.951
3.9 at.% Zn	3.6958	2.1602	3.3858	22.627	11.4362	45.8287
10.8 at.% Zn	2.0575	1.5324	1.2328	5.5621	5.8547	17.4972

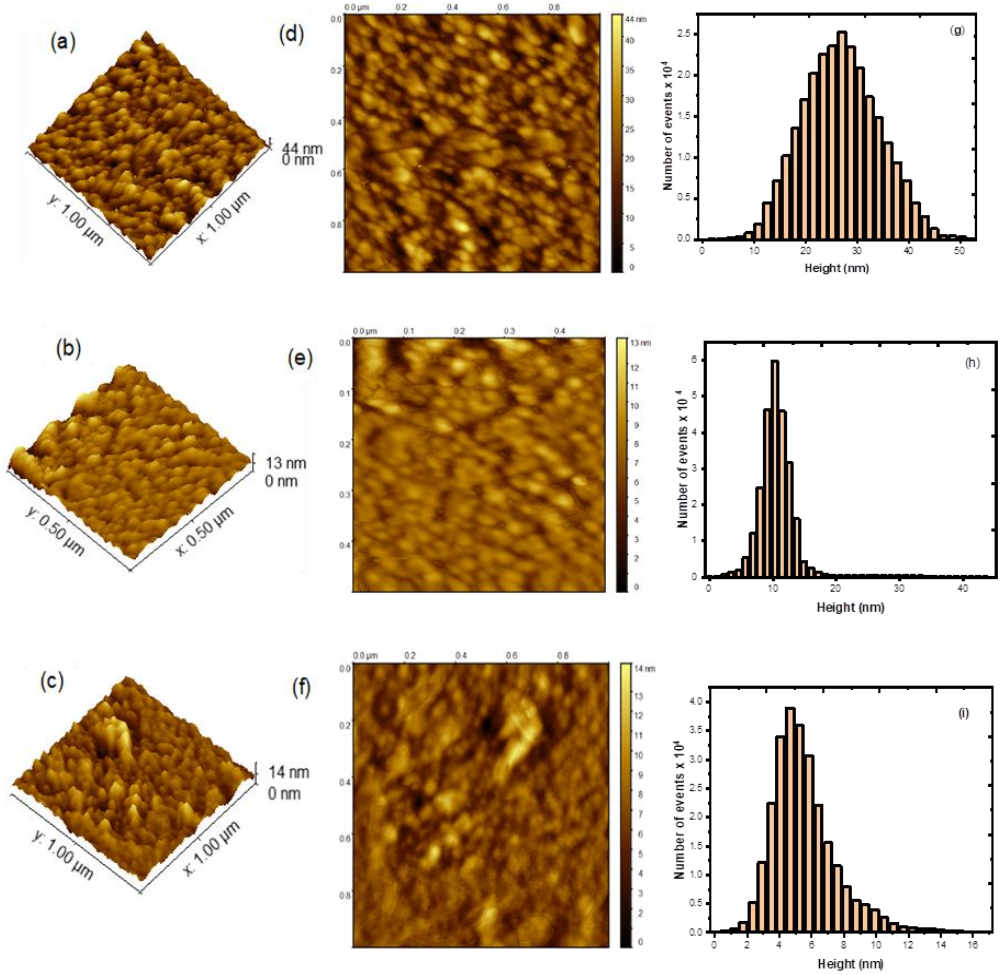

Figure 2: 3D and 2D AFM images with corresponding grain size distributions for W/Zn co-doped VO_2-based thin films with ~2.8 at.% Zn (a, d, g), ~3.9 at.% Zn (b, e, h) and ~ 10.8 at.% Zn (c, f, i) dopants concentrations.

RBS analysis of W/Zn co-doped VO_2-based thin films

Figure 3 (a), (b), and (c) presents RBS spectra of W/Zn co-doped VO_2-based thin films with their corresponding SIMNRA simulated spectra and Figure 3 (d) is the enlarged Zn contents spectra presented in Figure 3 (a), (b) and (c). All the spectra in Figure 3 confirmed the presence of vanadium (V), oxygen (O), tungsten (W) and zinc (Zn) in the samples. The spectra also indicated the presence of silicon (Si), which was thought to have originated from the soda lime glass (SLG) substrate. The dopant concentration of W was controlled at ~1.0 at.% W for all films and the influence of Zn dopant concentration on thermochromic properties of W/Zn co-doped VO_2 films was determined. Figure 3 (a) shows W/Zn co-doped VO_2-based thin films with the lowest dopant concentration at ~2.8 at.% Zn compared to ~3.9 at.% Zn and ~10.8 at% Zn from Figure 3 (b) and (c), respectively. A slight change in Zn concentration in the W/Zn co-doped VO_2-based thin films led to a significant change in the thermochromic properties of VO_2 films. Table 3 presents FWHM, counts as determined by Gaussian fit of the Zn peaks and the energy or channel in which the Zn peaks are situated. Information in Table 3

confirms the presence of different doping levels of Zn in the samples as shown in Figure 3. The sample with ~10.8 at% Zn was found to have slightly higher FWHM compared to that of ~3.9 at.% Zn and ~2.8 at.% Zn (Table 3). The counts or height in Figure 3 (d) gives the intensity or concentration of Zn dopant in the samples, and in this case, ~10.8 at% Zn, ~3.9 at.% Zn and ~2.8 at.% Zn were obtained, as summarized in Table 3.

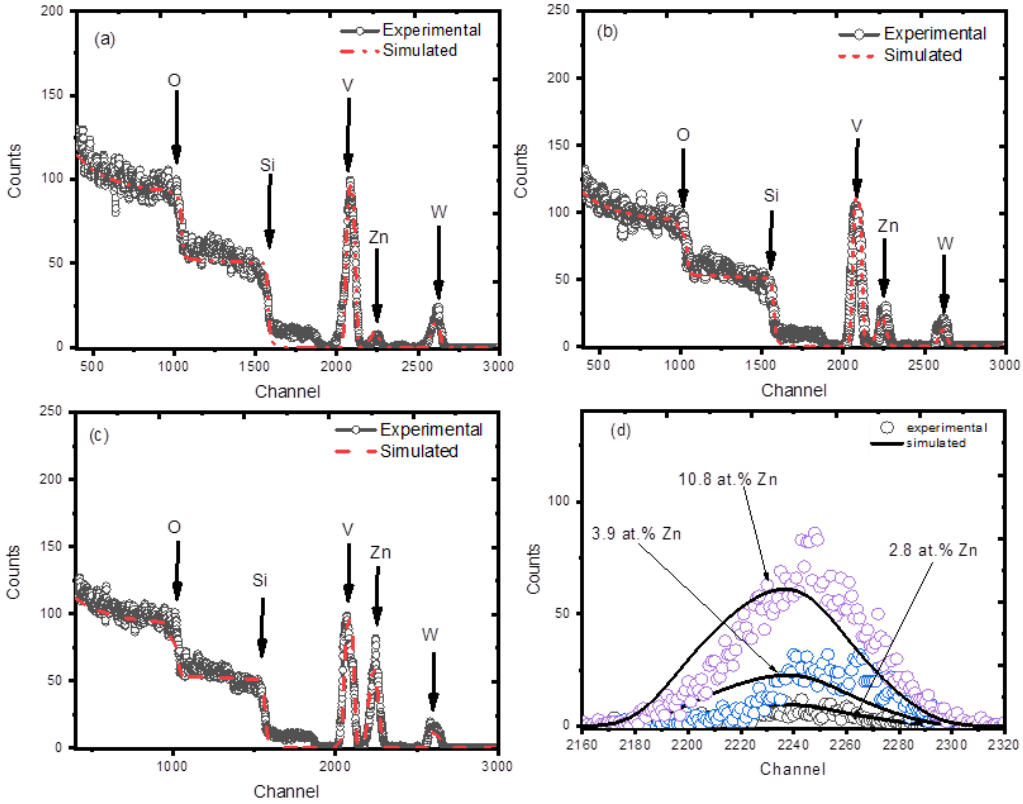

Figure 3: RBS data with SIMNRA spectra of W/Zn co-doped VO_2 thin films with different Zn concentrations of (a) 2.8 at.%, (b) 3.9 at.%, (c) 10.8 at.%, and (d) enlarged Zn peaks extracted from SIMNRA spectra in (a), (b) and (c).

Table 3: Full width at half maximum FWHM, counts (height), and peak position (channel) for the Zn peak

W/Zn co-doped VO_2 based thin films	FWHM	Counts (Height)	Peak position
~ 2.8 at.% Zn	54.57	2.11	2255.02
~3.9 at.% Zn	54.22	4.96	2256.6
~10.8 at% Zn	56.53	13.22	2255.7

Optical properties of W/Zn co-doped VO_2 based thin films

Figure 4 shows the spectral transmittance of the W/Zn co-doped VO_2-based thin films with different Zn dopant concentrations at room temperature and elevated temperature of 100 °C. In this case, W/Zn co-doped VO_2 thin film with ~2.8 at.% Zn showed a relatively higher peak transmittance of ~54.1% at the wavelength of 652 nm compared to 44.6% and 44.05% for the samples with ~3.9 at.% Zn and ~10.8 at.% Zn, respectively, around the same wavelength. All samples exhibited a decrease

in transmittance in the NIR region of the solar spectrum upon phase transition from the semiconducting phase at a lower temperature (below the critical temperature) to the metallic phase at higher temperature (above the critical temperature). Thus, a relatively higher NIR transmittance change at a wavelength of 2500 nm was observed at ~36.4% for W/Zn co-doped VO_2-based thin films with ~3.9 at.% Zn compared to 32.2% and 24% for the samples with ~10.8 at.% Zn and ~2.8 at.% Zn, respectively. Variations of solar and luminous transmittance modulation for W/Zn co-doped VO_2-based thin films are shown in Table 4. A thin film sample with ~2.8 at.% Zn showed slightly higher integrated luminous transmittance value of ~46% compared to 42% and 40% for the samples with ~3.9 at.% Zn and ~10.8 at.% Zn, respectively, and solar transmittance modulation was observed to be relatively higher for samples with higher Zn dopant concentration. An increase in Zn doping level to W/Zn co-doped VO_2 thin films might result to an increase in carrier concentrations of the samples as a result of increased oxygen vacancies. The increase in carrier concentration lowers the energy barriers between the semiconducting and metallic phases of VO_2 and hence the observed reduction in both the τ_c and the hysteresis loop width (Kang et al. 2021). With these results, it might be concluded that W and Zn dopants in VO_2-based thin film could be of potential in making these materials useful for smart windows applications.

Table 4: Variations of luminous and solar transmittances for W/Zn co-doped VO_2 based thin films

Zn doping level	$T_{lum,\ 25\ ^oC}$ (%)	$T_{lum,\ 100\ ^oC}$ (%)	$T_{sol,\ 25\ ^oC}$ (%)	$T_{sol,\ 100\ ^oC}$ (%)	ΔT_{sol} (%)
2.8 at.%Zn	46.11	44.47	42.05	38.07	3.97
3.9 at.%Zn	42.72	36.74	40.13	32.06	8.06
10.8 at.%Zn	40.40	35.33	41.59	31.38	10.20

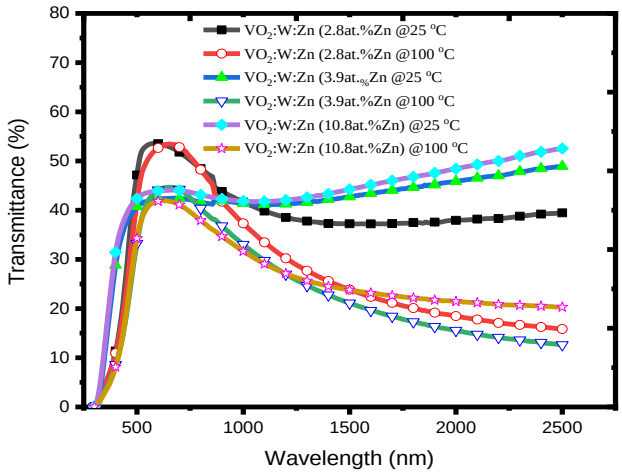

Figure 4: Spectral transmittance for W/Zn co-doped VO_2 thin films at 25 °C and 100 °C for different doping levels of Zn.

The temperature transmittance curves of the W/Zn co-doped VO_2 films with different doping levels of Zn at a wavelength of 2500 nm, together with their differential curve used to calculate the transition temperature are presented in Figure 5. At this wavelength region, the transmittance values for the films with 10.8 at.% Zn were relatively larger at

~53% compared to ~50% and ~40% for the thin films with 3.9 at.% Zn and 2.8 at.% Zn, respectively, in a semiconducting state. In a metallic state, the films showed lower transmittance values (Figure 5). The τ_c of the W/Zn co-doped VO_2-based thin films was found to decrease with an increase in the doping level of Zn, and consequently reduced the hysteresis loop width of the temperature–transmittance curves as shown in Figure 5.

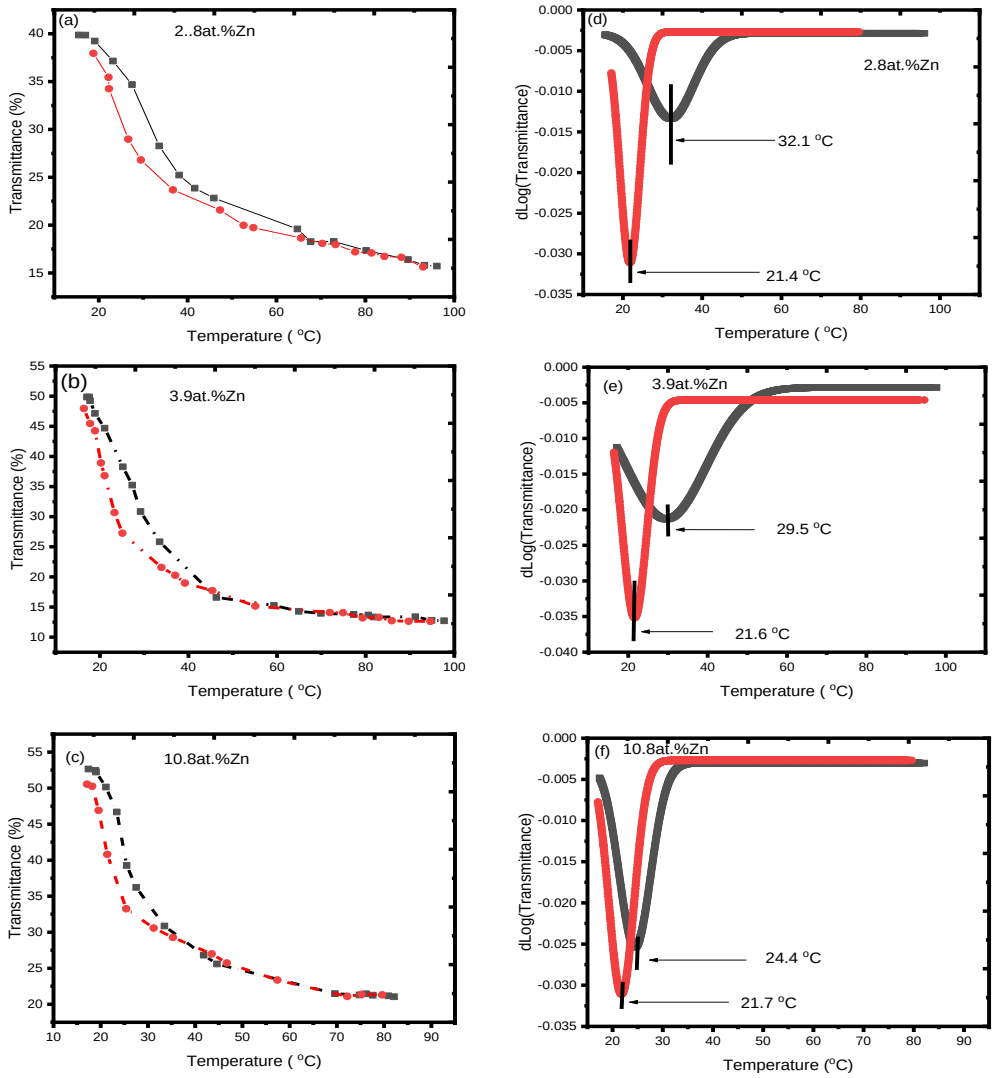

Figure 5: Transmittance-temperature curves of W/Zn co-doped VO_2 thin films with different Zn dopants of (a) 2.8 at.%, (b) 3.9 at.%, (c) 10.8 at.%, and their respective differential curves (d), (e) and (f).

Conclusion

W/Zn co-doped VO_2-based thin films with different Zn doping levels have been successfully prepared by DC magnetrons sputtering at a substrate temperature of 425 °C. The samples were characterised by XRD, AFM, RBS, and PerkinElmer lambda 1050+ UV/VIS/NIR spectrometer. W/Zn co-doped VO_2-based thin films with ~10.8 at.%Zn showed relatively lower τ_c of 23.1 °C compared to 25.6 °C and 26.8 °C for thin films with ~3.9 at.% Zn and ~2.8 at.% Zn,

respectively. The film's hysteresis loop widths were also found to decrease with increasing Zn contents. The τ_c reduction and hysteresis loop width reduction might be associated with an increase in carrier concentrations of the samples as a result of increased oxygen vacancies to the VO_2 based thin films. Furthermore, ΔT_{sol} of thin films with ~10.8 at.% Zn was relatively higher at ~10.2% as compared to ~8.06% and ~3.9% for films with ~3.9 at.% Zn and ~2.8 at.% Zn, respectively. On the other hand, thin films with ~2.8 at.% Zn possessed slightly higher luminous transmittance at 46.1% compared to 42.1% and 40.4% for films with ~3.9 at.% Zn and ~10.8 at.% Zn, respectively. The observed increases in Zn doping levels have resulted to smoother surface of VO_2 based thin films with smaller roughness values (Figure 2) that has led to reduced scattering and possibly increased NIR transmittance. This work revealed that an increase in the controlled amount of Zn in the W-doped VO_2 films improved ΔT_{sol} and decreased the τ_c. Furthermore, W and Zn inclusion in VO_2-based thin films with optimised amounts of W and Zn as dopants has the potential to significantly improve the thermochromic properties of VO_2-based thin films.

Conflicts of interest

The authors declare no conflict of interest.

Acknowledgement

H. F. Haji is grateful to the Ministry of Education Science and Technology (MoEST) Tanzania for PhD scholarship and The State University of Zanzibar (SUZA) for study leave. The International Science Program (ISP), The University of Dar es Salaam and National Research Foundation (NRF) iThemba LABS are acknowledged for financial support, research facilities and materials.

References

Batista C, Carneiro J, Ribeiro RM and Teixeira V 2011 Reactive pulsed-DC sputtered Nb-doped VO_2 coatings for smart thermochromic windows with active solar control. *J. Nanosci. Nanotechnol.* 11(10): 9042–9045.

Batista C, Ribeiro R, Carneiro J and Teixeira V 2009 DC sputtered w-doped VO_2 thermochromic thin films for smart windows with active solar control. *J. Nanosci. Nanotechnol.* 9(7): 4220–4226.

Burkhardt W, Christmann T, Franke S, Kriegseis W, Meister D, Meyer BK, Niessner W, Schalch D and Scharmann A 2002 Tungsten and flourine co-doping of VO_2 films. *Thin Solid Films* 402: 226–231.

Dou S, Zhang W, Wang Y, Tian Y, Wang Y, Zhang X, Zhang L, Wang L, Zhao J and Li Y 2018 A facile method for the preparation of W-doped VO_2 films with lowered phase transition temperature, narrowed hysteresis loops and excellent cycle stability. *Mater. Chem. Phys.* 215: 91–98.

Gagaoudakis E, Kortidis I, Michail G, Tsagaraki K, Binas V, Kiriakidis G and Aperathitis E 2016 Study of low temperature rf-sputtered Mg-doped vanadium dioxide thermochromic films deposited on low-emissivity substrates. *Thin Solid Films* 601: 99–105.

Granqvist CG, Green S, Niklasson GA, Mlyuka NR, Von Kraemer S and Georen P 2010 Advances in chromogenic materials and devices. *Thin Solid Films* 518(11): 3046–3053.

Guo H, Wang YG, Jain A, Fu HR and Chen FG 2021 Preparation of W/Zr co-doped VO_2 with improved microstructural and thermochromic properties. *J. Alloys Compd.* 878.

Haji HF and Mlyuka NR 2015 Optimization of spectral and angular selectivity in obliquely deposited TiO_2/Ag/TiO_2 thin films prepared by thermal evaporation and sputtering methods. *J. Mater. Sci. Eng. B.* 5(5-6): 206–221.

Haji HF, Numan N, Madiba IG, Mabakachaba B, Mtshali C, Khumalo Z, Kotsedi L, Mlyuka N, Samiji M and Maaza M 2023 Zn and W Co-doped VO_2-based thin films prepared by DC magnetron sputtering: Improved luminous transmittance and reduced transition

temperature. *J. Electron. Mater.* 52: 4020–4029.

Huang Z, Wu Z, Ji C, Dai J, Xiang Z, Wang D, Dong X and Jiang Y 2020 Improvement of phase transition properties of magnetron sputtered W-doped VO_2 films by post-annealing approach. *J. Mater. Sci. Mater. Electron.* 31(5): 4150–4160.

Ji C, Wu Z, Wu X, Wang J, Gou J, Huang Z, Zhou H, Yao W and Jiang Y 2018 Al-doped VO_2 films as smart window coatings: Reduced phase transition temperature and improved thermochromic performance. *Sol. Energy Mater. Sol.* 176: 174–180.

Kang J, Ryu J, Choi JG, Lee T, Park J, Lee S, Jang H, Jung YS, Kim KJ and Park BG 2021 Current-induced manipulation of exchange bias in IrMn/NiFe bilayer structures. *Nature Commun.* 12(1): 6420.

Karaoglan-Bebek G, Hoque MNF, Holtz M, Fan Z and Bernussi AA 2014 Continuous tuning of W-doped VO_2 optical properties for terahertz analog applications. *Appl. Phys. Lett.* 105(20)

Khan GR, Asokan K and Ahmad B 2017 Room temperature tunability of Mo-doped VO_2 nanofilms across semiconductor to metal phase transition. *Thin Solid Films* 625: 155–162.

Li SY, Mlyuka NR, Primetzhofer D, Hallén A, Possnert G, Niklasson GA and Granqvist CG 2013 Bandgap widening in thermochromic Mg-doped VO_2 thin films: Quantitative data based on optical absorption. *Appl. Phys. Lett*. 103 (16)

Li SY, Niklasson GA and Granqvist CG 2012 Thermochromic fenestration with VO_2-based materials: Three challenges and how they can be met. *Thin Solid Films* 520(10): 3823–3828.

Liu D, Cheng H, Xing X, Zhang C and Zheng W 2016 Thermochromic properties of W-doped VO_2 thin films deposited by aqueous sol-gel method for adaptive infrared stealth application. *Infrared Phys. Technol*. 77: 339–343.

Lyobha CJ, Mlyuka NR and Samiji ME 2018 Effects of aluminium and tungsten co-doping on the optical properties of VO_2 based thin films. *Tanz. J. Sci*. 44 (4): 91–99.

Mao Z, Wang W, Liu Y, Zhang L, Xu H and Zhong Y 2014 Infrared stealth property based on semiconductor (M)-to-metallic (R) phase transition characteristics of W-doped VO_2 thin films coated on cotton fabrics. *Thin Solid Films* 558: 208–214.

Mussa M, Mlyuka NR and Samiji ME 2018 Hall effect parameters of aluminium and tungsten co-doped VO_2 thin films. *Tanz. J. Sci*. 44(4): 100–105.

Mlyuka NR, Niklasson GA and Granqvist CG 2009 Thermochromic VO_2-based multilayer films with enhanced luminous transmittance and solar modulation. *Phys. Status Solidi: A.* 206(9): 2155–2160.

Mlyuka NR 2010 *Vanadium dioxide based thin films: Enhanced performance for smart window applications.* PhD thesis, University of Dar es Salaam.

Wang S, Liu M, Kong L, Long Y, Jiang X and Yu A 2016 Recent progress in VO_2 smart coatings: Strategies to improve the thermochromic properties. *Prog. Mater. Sci.* 81: 1–54.

Wang N, Liu S, Zhang XT, Magdassi S and Long Y 2015 Mg/W co-doped vanadium dioxide thin films with enhanced visible transmittance and low phase transition temperature. *J. Mater. Chem. C.:* 3(26): 6771–6777.

Yu Z, Liu Y, Zhang Z, Cheng M, Zou Z, Lu Z, Wang D, Shi J and Xiong R 2020 Controllable phase transition temperature by regulating interfacial strain of epitaxial VO_2 films. *Ceram. Int*. 46(8): 12393–12399.

Zhang Y, Li B, Wang Z, Tian S, Liu B, Zhao X, Li N, Sankar G and Wang S 2021 Facile preparation of $Zn_2V_2O_7$-VO_2 composite films with enhanced thermochromic properties for smart windows. *ACS Appl. Electron. Mater*. 3(5): 2224–2223.